Coastal Engineering 77 (2013) 49–56

Contents lists available at SciVerse ScienceDirect

Coastal Engineering

journal homepage: www.elsevier.com/locate/coastaleng

Growth of surface wind-waves in water of finite depth. A theoretical approach

P. Montalvo [a], J. Dorignac [a], M.A. Manna [a,*], C. Kharif [b,c], H. Branger [c]

[a] Université Montpellier 2, Laboratoire Charles Coulomb UMR 5221, F-34095, Montpellier, France
[b] Ecole Centrale Marseille, 38 rue Frédéric Joliot-Curie, 13451 Marseille cedex 20, France
[c] Institut de Recherche sur les Phénomènes Hors Équilibre, CNRS, AMU, UMR 7342, 49 rue Frédéric Joliot-Curie, BP 146, 13384 Marseille cedex 13, France

ARTICLE INFO

Article history:
Received 23 October 2012
Received in revised form 6 February 2013
Accepted 15 February 2013
Available online 19 March 2013

Keywords:
Wind-generated waves
Wind-waves growth rates
Miles' theory

ABSTRACT

The Miles' theory of wave amplification by wind is extended to the case of finite depth. A depth-dependent wave growth rate is derived from the dispersion relation of the wind/water interface. For different values of the dimensionless water depth parameter $\delta = gh/U_1^2$, with h the depth, g the gravity and U_1 a characteristic wind speed, a family of wave growth curves is plotted as a function the dimensionless parameter $\theta_{fd} = \frac{c}{U_1}$, with c the wave phase velocity. The model provides a fair agreement with the data and empirical relationships obtained from the Lake George experiment, as well as with the data from the Australian Shallow Water Experiment. Two major results are obtained: (i) for small θ_{fd} the wave growth rates are comparable to those of deep water and (ii) for large θ_{fd} a finite-depth limited growth is reached, with wave growth rates going to zero.

1. Introduction

1.1. Field experiments on growth of surface wind-waves

Experimental studies on the growth rate of surface wind-waves under fetch or wave age limited conditions in deep or finite water depth is a classical matter of investigation in fluid dynamics.

For finite depth wave growth the pioneer experiments and numerical studies were conducted by Thijsse (1949), Bretschneider (1958) and Ijima and Tang (2011) and particularly the experiments in Lake George, Australia, described by Young and Verhagen (1996a). They provided one of the first systematic attempts to understand the physics of wind-wave generation in finite depth water.

The results of the field experiments in fetch limited growth have been presented in references Young and Verhagen (1996a, 1996b) and Young and Babanin (2006a). These papers gave a very complete description of the basin geometry and bathymetry, experimental design, used instrumentation, as well as the adopted scaling parameters. The measurements have confirmed the water depth dependence of the asymptotic limits to wave growth.

In Young (1997) (see Young (1999), too) derived was an empirical relation in terms of appropriate dimensionless parameters, which able to reproduce the experimental data of Young and Verhagen (1996a). In particular the empirical relationship between the variation of fractional energy and the inverse wage age, found by Donelan et al. (1992) for deep water, was extended to the finite depth domain. Experimental results together with plots of the empirical laws have shown that, contrary to the deep water case, the wave age at which the growth rate becomes zero is wind-dependent and depth-dependent. So, the case of a fully-developed sea is warped from the deep water case, as it was established by Pierson and Moskowitz (1964). As a result, a growth law against the inverse wave age exists for each value of a parameter, which involves the dependence on wind intensity and water depth.

The evolution of the growth rates is such that at small wave ages growth rates are comparable to the deep water limit and at large wave ages the growth rate is lower in shallow water than in deep water. Beyond a critical wave age, the growth rate vanishes.

1.2. Theoretical studies

From a theoretical point of view pioneering surface wind-wave growth theories have been developed since Jeffreys (1924, 1925), Phillips (1957) and Miles (1957) until more recent works of Janssen (1991) and Belcher and Hunt (1993). Later on, numerical approaches were used. For a review one can refer to the book of Janssen (2004).

Nonetheless, most of these theories are limited to the deep water domain, thus restrictive with regard to wind generated near-shore ocean waves or shallow lake waves. Nowadays we do not have any consistent theoretical framework to forecast growth of wind-waves in finite water depth. Therefore a theoretical extension of wave growth to finite depth is lacking in the field.

* Corresponding author. Tel.: +33 467143219.
E-mail addresses: pablo.montalvo@univ-montp2.fr (P. Montalvo), miguel.manna@univ-montp2.fr (J. Dorignac), jerome.dorignac@univ-montp2.fr (M.A. Manna), christian.kharif@centrale-marseille.fr (C. Kharif), branger@irphe.univ-mrs.fr (H. Branger).

0378-3839/$ – see front matter © 2013 Elsevier B.V. All rights reserved.
http://dx.doi.org/10.1016/j.coastaleng.2013.02.008

The aim of this work is to derive a surface wind-wave growth theory in finite depth based on the Euler equations. The purpose is twofold: (i) to provide mathematical laws able to qualitatively reproduce some features of the field experiments on growth rate evolution of finite depth wind-waves, and (ii) to supply a theoretical basis allowing to it go beyond empirical laws.

To carry out this task, we propose to extend the well known Miles' theory to the case of finite depth. The paper is organized as follows.

In Section 2 we briefly introduce the classical Miles' theory. In sub-section 3.1 the linear problem in water is displayed. Then, in sub-section 3.2 air and water dynamics are coupled. The linear problem is solved at the interface and the linear dispersion relation of wave amplification in finite depth is derived. In Section 4 we introduce dimensionless variables and scalings, to obtain an adequate growth rate and in sub-section 1 we derive the β-Miles parameter in finite depth. The theoretical linear dynamic is discussed in sub-section 4.2. In sub-section 5.1 the theoretical laws are compared with the Young–Verhagen data and plot of empirical relationships from the Lake George experiment and Donelan's data from the AUSWEX program with a special emphasis on their qualitative agreement. In sub-section 5.2 discussed is the wave dissipation due to white-capping. Finally section 6 draws the conclusions. Besides, in Appendix A we give some details about the numerical work underneath.

2. Miles' theory of wind-wave growth in deep water: a brief summary

From a mathematical point of view, the classical Miles' theory in deep water is based on the dispersion relation of the air–sea interface and the related Rayleigh equation (Conte and Miles, 1959; Drazin and Reid, 1982; Rayleigh, 1880). Miles' physical mechanism of wave generation by wind assumes that ocean surface waves are generated by a resonance phenomenon between the wave-induced pressure gradient in the inviscid shear airflow and the surface waves. It occurs at the critical height, or matched height, where the air flow velocity is equal to the phase speed of the surface wave. The usual model is two-dimensional, water is assumed deep, viscosity in air and water is disregarded and the equations of motion are linearized. The equations are linearized around a prescribed mean wind velocity and air flow turbulence is only used to set up the mean wind profile. The subsequent Rayleigh equation, depending on the wind profile, is then solved by a combination of analytical and numerical methods.

Despite these simplifications, this theory provides an approximate model sufficiently useful to investigate some of the physics of the water wave growth problem. This model allows, at least linearly, an analytical approach of the phenomenon. Its prediction of exponential growth of wave amplitude (or energy) is well confirmed by field and laboratory experiments (the wind-to-waves energy transfer rates predictions are smaller than the observations, although their order of magnitude is the same). Even though the Miles' theory is very well-argued from the mathematical point of view and under the assumptions used, it has been largely improved, lately.

For a detailed review on wind-induced wave growth as well as improvements of the linear Miles' theory and further progress in the quasi linear theory see Miles (1997) and Janssen (2004).

3. The interface problem

This section is devoted to the study of the stability of an air–water interface. Let the fluid particles be located relatively to a fixed rectangular Cartesian frame with origin O and axes (x, y, z), where Oz is the upward vertical direction. We assume translational symmetry along y and we will only consider a sheet of fluid parallel to the xz plane. The plane $z = 0$ characterizes the interface at rest. The perturbed air–water interface will be described by $z = \eta(x, t)$. The air occupies the $\eta(x, t) < z < +\infty$ region, and the water lies between the bottom located at $z = -h$ and the interface $z = \eta(x, t)$. We suppose the water as well as the air to be inviscid and incompressible. The unperturbed air flow is a prescribed mean shear flow, only depending on the vertical coordinate z. We assume the dynamics to be linear, and disregard the air flow turbulence, building a *quasi-laminar theory*.

3.1. The water domain

In the water domain we consider the Euler equations for finite depth. The horizontal and vertical velocities of the fluid are $u(x, z, t)$, and $w(x, z, t)$, respectively. The continuity equation and linearized equations of motion in water read as (Lighthill, 1978)

$$u_x + w_z = 0, \quad \rho_w u_t = -P_x, \quad \rho_w w_t = -P_z - g\rho_w, \tag{1}$$

where $P(x, z, t)$ is the pressure, g the gravitational acceleration, ρ_w the water density and subscripts in u, w and P denote partial derivatives. The boundary conditions at $z = -h$ and at $z = \eta(x, t)$ are

$$w(-h) = 0, \quad \eta_t = w(0), \tag{2}$$

$$P(x, \eta, t) = P_a(x, \eta, t), \tag{3}$$

where P_a is the air pressure evaluated at $z = \eta$. Thus Eq. (3) is the continuity of the pressure across the air/water interface. As this is a vital assumption for the growth mechanism, we express the pressure in a more manageable reduced form defined by

$$\mathbf{P}(x, z, t) = P(x, z, t) + \rho_w g z - P_0, \tag{4}$$

where P_0 is the atmospheric pressure. In terms of Eq. (4), Eqs. (1)–(3) read

$$u_x + w_z = 0, \quad \rho_w u_t = -\mathbf{P}_x, \quad \rho_w w_t = -\mathbf{P}_z, \tag{5}$$

$$w(-h) = 0, \quad \eta_t = w(0), \tag{6}$$

$$\mathbf{P}(x, \eta, t) = P_a(x, \eta, t) + \rho_w g \eta - P_0. \tag{7}$$

The linear system Eqs. (5)–(7) can be solved by assuming normal mode solutions of the form

$$\begin{aligned} \mathbf{P} &= \mathcal{P}(z)\exp(i\theta), \quad u = \mathcal{U}(z)\exp(i\theta), \\ w &= \mathcal{W}(z)\exp(i\theta), \quad \eta = \eta_0 \exp(i\theta), \end{aligned} \tag{8}$$

with $\theta = k(x - ct)$ where k is the wavenumber, c the phase speed and η_0 a constant. Using Eqs. (5)–(8) we obtain

$$w(x, z, t) = \frac{ikc \sinh k(z + h)}{\sinh kh} \eta_0 \exp(i\theta), \tag{9}$$

$$u(x, z, t) = \frac{kc \cosh k(z + h)}{\sinh kh} \eta_0 \exp(i\theta), \tag{10}$$

$$\mathbf{P}(x, z, t) = \frac{k\rho_w c^2 \cosh k(z + h)}{\sinh kh} \eta_0 \exp(i\theta). \tag{11}$$

The phase speed c is unknown in Eqs. (9)–(11). To determine c we have to consider the boundary conditions (7), not yet used, and Eq. (6) which yields

$$\rho_w \eta_0 \exp(i\theta)\left\{c^2 k \coth kh - g\right\} + P_0 = P_a(x, \eta, t). \tag{12}$$

In the single-domain problem $P_a(x, \eta, t) = P_0$ and Eq. (12) gives the usual expression for c,

$$c^2 = c_0^2 = \frac{g}{k} \tanh(kh). \tag{13}$$

Note that it is not the case in the problem under consideration. In the present paper the determination of c needs the use of the air pressure evaluated at $z = \eta$.

3.2. The air domain

Let us consider the linearized governing equation of a steady air flow, with a prescribed mean horizontal velocity $U(z)$ depending on the vertical coordinate z. We are going to study perturbations to the mean flow $U(z)$: $u_a(x, z, t)$, $w_a(x, z, t)$ and $P_a(x, z, t)$ where subscript a stands for *air*. So with $\mathbf{P}_a(x, z, t) = P_a(x, z, t) + \rho_a g z - P_0$, ρ_a, the air density, and $U' = dU(z)/dz$ we have the following equations

$$u_{a,x} + w_{a,z} = 0, \tag{14}$$

$$\rho_a\left[u_{a,t} + U(z)u_{a,x} + U'(z)w_a\right] = -\mathbf{P}_{a,x}, \tag{15}$$

$$\rho_a\left[w_{a,t} + U(z)w_{a,x}\right] = -\mathbf{P}_{a,z}. \tag{16}$$

To these equations we must add the appropriate boundary conditions. The first one is the kinematic boundary condition for air, evaluated at the aerodynamic sea surface roughness z_0, located just above the interface. Through this paper, z_0 will be assumed constant, independent from the sea state. This is a widely used approximation, first proposed by Charnock (1955). For the datasets used later on, the wind speed ranges are such that the roughness may be seen as a constant (Fairall et al., 1996). The kinematic boundary condition reads

$$\eta_t + U(z_0)\eta_x = w_a(z_0). \tag{17}$$

We choose $U(z)$ to be the logarithmic wind profile

$$U(z) = U_1 \ln(z/z_0), \quad U_1 = \frac{u_*}{\kappa}, \quad \kappa \approx 0.41, \tag{18}$$

where u_* is the friction velocity and κ the Von Kármán constant. This is commonly used to describe the vertical distribution of the horizontal mean wind speed within the lowest portion of the air-side of the marine boundary layer (Garratt et al., 1996). It can also be justified with scaling arguments and solution matching between the near-surface air layer and the geostrophic air layer (see Tennekes (1972)). So, Eq. (17) can be reduced to

$$\eta_t = w_a(z_0). \tag{19}$$

Next we assume $\mathbf{P}_a = \mathcal{P}_a(z)\exp(i\theta)$, $u_a = \mathcal{U}_a(z)\exp(i\theta)$, $w_a = \mathcal{W}_a(z)\exp(i\theta)$, and we add the following boundary conditions on $\mathcal{W}_a$ and $\mathcal{P}_a$,

$$\lim_{z\to+\infty}(\mathcal{W}_a' + k\mathcal{W}_a) = 0 \tag{20}$$

$$\lim_{z\to z_0}\mathcal{W}_a = W_0, \tag{21}$$

$$\lim_{z\to+\infty}\mathcal{P}_a = 0, \tag{22}$$

that is, the disturbance plus its derivative vanish at infinity, and the vertical component of the wind speed is enforced by the wave movement at the sea surface. Then, using Eqs. (14)–(16) and (22) we obtain

$$w_a(x, z, t) = \mathcal{W}_a\exp(i\theta), \tag{23}$$

$$u_a(x, z, t) = \frac{i}{k}\mathcal{W}_{a,z}\exp(i\theta), \tag{24}$$

$$\mathbf{P}_a(x, z, t) = ik\rho_a\exp(i\theta)\int_z^\infty [U(z') - c]\mathcal{W}_a(z')dz'. \tag{25}$$

Removing the pressure from the Euler equations, we obtain the well-known Rayleigh equation (Rayleigh, 1880), $\forall z \backslash z_0 < z < +\infty$

$$(U - c)\left(\mathcal{W}_a'' - k^2\mathcal{W}_a\right) - U''\mathcal{W}_a = 0, \tag{26}$$

which is singular at the critical, or matched height $z_c = z_0 e^{c\kappa/u_*} > z_0 > 0$, where $U(z_c) = c$. We recall that this model disregards any kind of turbulence, and so that the critical height is set above any turbulent eddies or other non-linear phenomena. In Eqs. (23)–(26) neither $\mathcal{W}_a(z)$ nor c are known. In order to find c, we have to calculate $P_a(x, \eta, t)$. We obtain

$$P_a(x, \eta, t) = P_0 - \rho_a g\eta + ik\rho_a\exp(i\theta)\int_{z_0}^\infty [U(z) - c]\mathcal{W}_a(z)dz, \tag{27}$$

where the lower integration bound is taken at the constant roughness height z_0 instead of $z = \eta$ since we are studying the linear problem. Finally, using Eq. (19) to eliminate the term $ik\rho_a\exp(i\theta)$ and substituting P_a given by Eq. (27) into Eq. (12) gives

$$g(1 - s) + c\frac{sk^2}{W_0}I_1 - c^2\left\{\frac{sk^2}{W_0}I_2 + k\coth(kh)\right\} = 0, \tag{28}$$

where $s = \rho_a/\rho_w$ and the integrals I_1 and I_2 are defined as follows

$$I_1 = \int_{z_0}^\infty U\mathcal{W}_a dz, \quad I_2 = \int_{z_0}^\infty \mathcal{W}_a dz. \tag{29}$$

Eq. (28) is the dispersion relation of the problem. When $h \to \infty$ we find the expression derived by Beji and Nadaoka (2004) (see equation (3.7)). The parameter s being small ($\rho_a/\rho_w \sim 10^{-3}$) Eq. (28) may be approximated as

$$c = c_0 + sc_1 + O\left(s^2\right). \tag{30}$$

The explicit form of c_1 is calculated in the next section. At order zero in s, we can find $\mathcal{W}_a(z)$ by using c_0 instead of c and solving Eq. (26). The method is shortly described in Appendix A.

4. The wave growth rate γ

The function $\mathcal{W}_a(z)$ is complex and consequently c, too. Its imaginary part gives the growth rate of $\eta(x, t)$ defined by

$$\gamma = k\Im(c) \tag{31}$$

where $\Im(c)$ is the imaginary part of c. The theoretical and numerical results concerning the growth rate γ are studied and computed with two dimensionless parameters δ (see Young and Verhagen 1996a,b) and θ_{dw} defined by

$$\delta = \frac{gh}{U_1^2}, \quad \theta_{dw} = \frac{1}{U_1}\sqrt{\frac{g}{k}}. \tag{32}$$

The dimensionless parameter δ, for constant U_1, measures the influence of the depth on the rate of growth of $\eta(x, t)$. The parameter θ_{dw} can be seen as a *theoretical analogous of the deep water wave age*. It measures the relative value of the deep water phase velocity to the characteristic wind velocity U_1. Now a *theoretical analogous of the finite depth wave age* θ_{fd} can be introduced as

$$\theta_{fd} = \frac{1}{U_1}\sqrt{\frac{g}{k}}\sqrt{\tanh(kh)} = \theta_{dw}T^{1/2}, \tag{33}$$

where

$$T = \tanh\left(\frac{\delta}{\theta_{dw}^2}\right). \tag{34}$$

The form (33) is a depth weighted parameter such that for a finite and constant θ_{dw} we have $\theta_{fd} \sim \theta_{dw}$ if $\delta \to \infty$ and $\theta_{fd} \sim \delta^{1/2} = \sqrt{gh}/U_1$ if $\delta \to 0$. To derive the growth rate, we introduce the following dimensionless variables and scalings (hats meaning dimensionless quantities)

$$U = U_1\hat{U}, \quad \mathcal{W}_a = W_0\hat{\mathcal{W}}_a, \quad z = \frac{\hat{z}}{k}, \qquad c = U_1\hat{c}, \quad t = \frac{U_1}{g}\hat{t}. \tag{35}$$

Using Eqs. (32) and (35) in Eq. (28) and retaining only the terms of order $\mathcal{O}(s)$ we obtain $\hat{c}$,

$$\hat{c} = \hat{c}(\delta, \theta_{dw}) = \theta_{dw}T^{1/2} - \frac{s}{2}\theta_{dw}T^{1/2} + \frac{s}{2}\left\{T\hat{I}_1 - \theta_{dw}T^{3/2}\hat{I}_2\right\}, \tag{36}$$

and with $e^{\gamma t} = e^{k\Im(c)t} = e^{\Im(\hat{c})\hat{t}}/\theta_{dw}^2$, we derive the dimensionless growth rate $\hat{\gamma} = \frac{U_1}{g}\gamma$,

$$\hat{\gamma} = \frac{s}{2}\left\{\frac{T\Im(I_1)}{\theta_{dw}^2} - \frac{T^{3/2}\Im(I_2)}{\theta_{dw}}\right\}. \tag{37}$$

Hence, we can compute $\hat{\gamma}$ for given values of δ and θ_{dw}. The δ parameter does not appear explicitly allowing us to indeed compute $\hat{\gamma}$ for an infinite depth. For $\delta \to \infty$, we have

$$\hat{\gamma} = \frac{s}{2}\left\{\frac{\Im(I_1)}{\theta_{dw}^2} - \frac{\Im(I_2)}{\theta_{dw}}\right\}. \tag{38}$$

This is exactly the expression found by Beji and Nadaoka (2004) for deep water.

4.1. The β-Miles parameter

Instead of dimensionless growth rate $\hat{\gamma}$, Miles introduced β as a non-dimensional parameterization of the imaginary part, $\Im(c)$, of the phase velocity depending on the air–water densities ratio s and friction velocity u_* ($U_1 = u_*/\kappa$)

$$\Im(c) = c_0\frac{s}{2}\beta\left(\frac{U_1}{c_0}\right)^2, \tag{39}$$

with c_0 the wave phase velocity. Using Eq. (31) we have

$$c_0\frac{s}{2}\beta\left(\frac{U_1}{c_0}\right)^2 = \frac{\gamma}{k} = \frac{g\hat{\gamma}}{kU_1}, \tag{40}$$

then, dividing by U_1 we get the following dimensionless relation

$$\theta_{dw}^2\hat{\gamma} = \frac{s}{2}\beta\frac{1}{\theta_{fd}} \tag{41}$$

that gives the transformation rule between the Miles' parameter β and dimensionless growth rate $\hat{\gamma}$

$$\beta = \frac{2\hat{\gamma}}{s}\theta_{dw}^3T^{1/2}. \tag{42}$$

This is a straightforward definition of Miles' β in finite depth.

4.2. The $\hat{\gamma}$ and β curves

In contrast to the usual analysis of wind-wave growth, our results concern the dimensionless growth rate $\hat{\gamma}$ instead of the β-Miles parameter. The existence of a finite depth h transforms the unique curve of wave growth rate in deep water into a *family of curves*, a curve corresponding to a fixed value of $\delta = gh/U_1^2$. In Fig. 1 is shown a family of six values of $\hat{\gamma}$ as a function of θ_{fd}, for fixed values of the parameter δ. The curve corresponding to $\delta \to \infty$ is plotted as well.

- Fig. 1 shows that at small θ_{fd} the growth rates $\hat{\gamma}$ become equal for all the values of δ, the limit corresponds to the deep water case. Note that small finite values of θ_{fd} defines young surface waves. This stage represents the initial growth of the wave field of a calm lake, for instance.
- When time increases, the surface waves reach moderate values of θ_{fd} that correspond to mild or moderate wave ages. As θ_{fd} increases, finite-depth effects start to occur. The growth rate becomes lower than in deep water. For a given value of θ_{fd}, the dimensionless growth rate $\hat{\gamma}$ increases as δ increases.
- Old waves are found for large values of θ_{fd} and correspond to small $\hat{\gamma}$ values.

As $\hat{\gamma}$ goes to zero, each δ-curve approaches a (idealized) *theoretical θ_{fd}-limited growth*. At this stage the wave reaches a final state of linear progressive wave with no growth. In others words waves with ages older than a critical wave age (corresponding to $\hat{\gamma} \to 0$) are no more amplified.

The β parameter evolution as a function of θ_{fd} is shown in Fig. 2, displaying the correct deep water trend, and the new finite depth limits. The effect of depth is critical. β shows little variation for small values of θ_{fd}, as usual, but it goes dramatically to zero when θ_{fd} is increased. From a physical point of view Fig. 1 (or Fig. 2) is a snapshot of the theoretical dynamical development of a wave which is growing both in amplitude and wave age.

5. Theoretical laws and qualitative comparisons with field experiments

This section is aimed at showing that our analytical and numerical results are able to qualitatively reproduce some experimental results. It is important to have in mind two facts: firstly, we are studying linear growth of a normal Fourier mode and not the growth of a wave train as the infinite superposition of wave Fourier modes, and secondly, the only physical active process we have considered is the atmospheric input.

5.1. Theoretical equivalents of experimental parameters

Results in field or laboratory experiments are commonly given using the parameter C_p, the observed phase speed at the peak frequency ω_p. Consequently, qualitative comparison with field observations can only be done using the phase velocity c or frequency ω of one mode instead of C_p or ω_p.

First of all we are going to show that the theoretical curves for $\hat{\gamma}$ are, *mutatis mutandi*, in good qualitative agreement with the empirical curves of the dimensionless fractional wave energy increase per radian $\hat{\Gamma}$ as a function of the inverse wave age U_{10}/Cp, given in Young (1997). In this paper, experimental field data for $\hat{\Gamma}$ in the finite depth Lake George are adequately represented by the empirical relationship (Eq. (6) in reference above)

$$\hat{\Gamma} = \frac{C_g}{\omega_p}\frac{1}{E}\frac{\partial E}{\partial x} = A\left(\frac{U_{10}}{C_p} - 0,83\right)\tanh^{0,45}\left(\frac{U_{10}}{C_p} - \frac{1,25}{\delta_Y^{0.45}}\right), \tag{43}$$

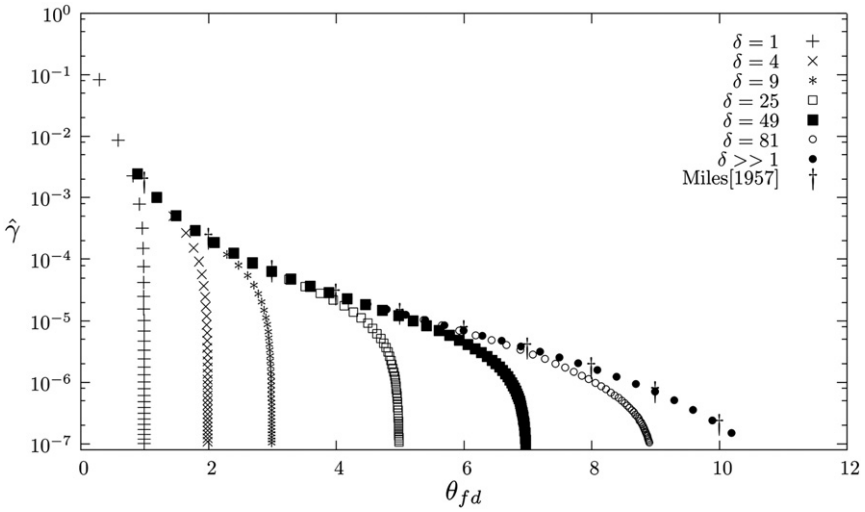

Fig. 1. Evolution of the growth rate in semi-logarithmic scale. Every curve but the rightmost one corresponds to finite depth. From left to right, they match $\delta = 1,4,9,25,49,81$. We can observe that for each depth, there is a θ_{fd}-limited wave growth. The deep water limit, also computed, is corresponds to small θ_{fd} and matches Miles' results.

with A constant, $\delta_Y = gh/U_{10}^2$ the non-dimensional water depth, U_{10} the wind velocity at 10 m, and C_g and C_p the group and phase speeds of the components at the spectral peak frequency ω_p.

To make a qualitative comparison between $\hat{\Gamma}$ curves as functions of the inverse wave-age U_{10}/C_p and theoretical $\hat{\gamma}$ curves as functions of $1/\theta_{fd}$ we need to write the empirical $\hat{\Gamma}$ in terms of theoretical quantities. Hence, the following changes are necessary:

$$\text{measured} \quad C_g, C_p, \omega_p \rightarrow \quad \text{theoretical} \quad c_g, c, \omega, \tag{44}$$

$$\frac{U_{10}C_{10}^{1/2}}{\kappa} = u_*/\kappa = U_1, \tag{45}$$

with C_{10} the 10 m drag coefficient (Wu, 1982). Thus, noting that the energy growth rate is two times the amplitude growth rate, that is

$$\Gamma = 2\gamma,$$

and using $2c_g = c(1 + 2kh/\sinh(2kh))$, Eqs. (44), (45),(33) and (35), we obtain

$$\hat{\Gamma} = \frac{\theta_{dw}}{T^{1/2}}\hat{\gamma}\left[1 + \frac{2\delta}{\theta_{dw}^2 \sinh\left(\frac{2\delta}{\theta_{dw}^2}\right)}\right]. \tag{46}$$

This expression gives the theoretical equivalent of the empirical $\hat{\Gamma}$ as a function of θ_{dw}, δ and $\hat{\gamma}$. The values of $\hat{\gamma}$ as a function of $1/\theta_{fd}$ for fixed values of δ are numerically computed from Eqs. (33), (34) and (37). Steps (44) and (45) transform δ_Y and C_p/U_{10} into δ and θ_{fd} according to

$$\delta_Y = \delta\frac{C_{10}}{\kappa^2}, \tag{47}$$

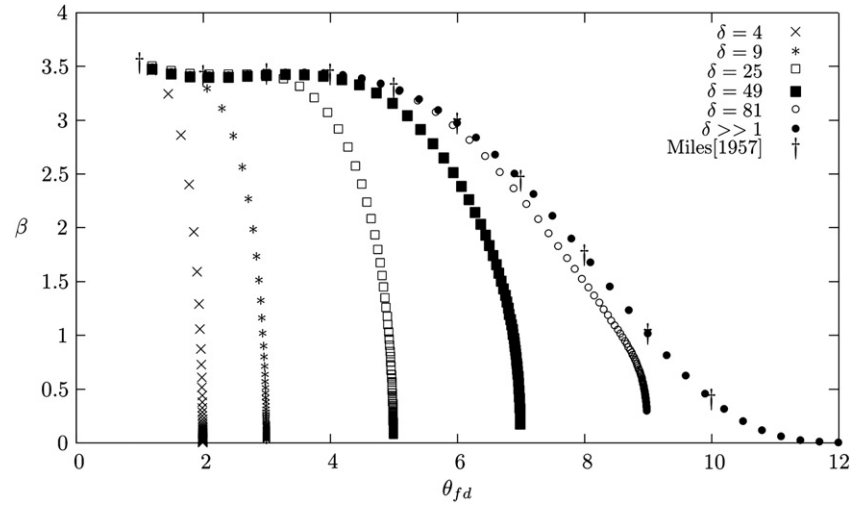

Fig. 2. Evolution of Miles' coefficient β for several values of the depth. Each curve is plotted with the same Charnock constant $\alpha_c \approx 0.018$. The finite-depth effect is critical, and high value of δ correspond to deep water.

$$\frac{C_p}{U_{10}} = \theta_{fd}\frac{C_{10}^2}{\kappa}. \tag{48}$$

In Young (1997) the curves of $\hat{\Gamma}_Y$ versus U_{10}/C_p have been presented for the δ_Y-ranges, $\delta_Y \in [0.1 - 0.2],[0.2 - 0.3],[0.3 - 0.4],[0.4 - 0.5]$, rather than for a single value of δ_Y. The intervals were determined from the variations in U_{10}, the depth h being nearly constant, close to 2 m. Consequently we substitute the δ_Y-ranges with δ-ranges using Eq. (47) and we compute the mean value $< \delta >$. For example in Fig. 3(a), $\delta_Y \in [0{,}1 - 0{,}2]$ is transformed into $\delta = [13{,}17 - 26{,}35]$ with $< \delta > = 19{,}76$. Fig. 3(a), (b), (c) and (d) shows a fair agreement between the model and the experimental data and plots of empirical laws for Lake George. The agreement improves as $\frac{1}{\theta_{fd}}$ increases.

In Fig. 4 plotted, against δ, are the critical values of the parameter θ_{fd}^c for which the growth rate γ goes to zero. They obey the relation

$$\theta_{fd}^c = \delta^{0.5}. \tag{49}$$

The above relation, found numerically, is coherent with the parameter formulation Eq. (33). It is indeed a limiting value for θ_{fd} uniquely determined by the water depth. Young (1997) found empirically a relationship (Eq. (6)) showing the existence of a limit to growth when the inverse wave age satisfies the following expression

$$\frac{C_p}{U_{10}} = 0.8\left(\frac{gh}{U_{10}^2}\right)^{0.45}. \tag{50}$$

This relationship corresponds to growth rate $\hat{\Gamma}$ going to zero. Using a C_{10} drag coefficient parameterization such as (Wu, 1982)

$$C_{10} = (0.065U_{10} + 0.8)10^{-3}, \tag{51}$$

and taking an average $U_{10} = 7m/s$ in Young (1997), one finds the U_1 to U_{10} relationship

$$U_{10} \approx 28,3\, u_* \approx 11,6\, U_1, \tag{52}$$

So, this depth limited state reads

$$\frac{C_p}{U_1} = 1,01\delta^{0.45}. \tag{53}$$

A result in excellent agreement with the theoretical value Eq. (49). With θ_{fd}^c we can calculate the corresponding critical wave length λ^c. Substituting Eq. (49) into Eq. (33) we obtain

$$\frac{\delta}{\theta_{dw}^2} = \tanh\left(\frac{\delta}{\theta_{dw}^2}\right). \tag{54}$$

Eq. (54) means that the wave is meeting a shallow water zone. In such a limit, the range of δ/θ_{dw}^2 is: $0 < \delta/\theta_{dw}^2 < \frac{\pi}{4}$ (Fenton (1979), Francius and Kharif (2006)). As a result we get $\lambda^c = 8$ h. For values of λ such that $\lambda > \lambda^c$ the phase velocity is in the long wave limit i.e., $c = \sqrt{gh}$. Consequently, if $\lambda > \lambda_c$ the wave feels the bottom, the amplitude does not grow anymore, the wind-wave resonance mechanism ceases, and the wave reaches its utmost state as a progressive plane wave.

Finally in Fig. 4 are also plotted data of Donelan et al. (2006), from the Australian Shallow Water Experiment. A fit is also plotted to show the trend. The raw data consists in the water depth h in meters, the friction velocity u_*, the wind velocity U_{10} and the ratio U_{10}/C_p where c_p is the measured phase velocity. For example, $u_* = 0.44$ m s^{-1} and $h = 0.32$ m give $\delta = 2.7$ and $\theta_{fd} = 1.55$, which satisfy Eq. (49) with small error. All the points (δ,θ_{fd}) are close to the theoretical limit.

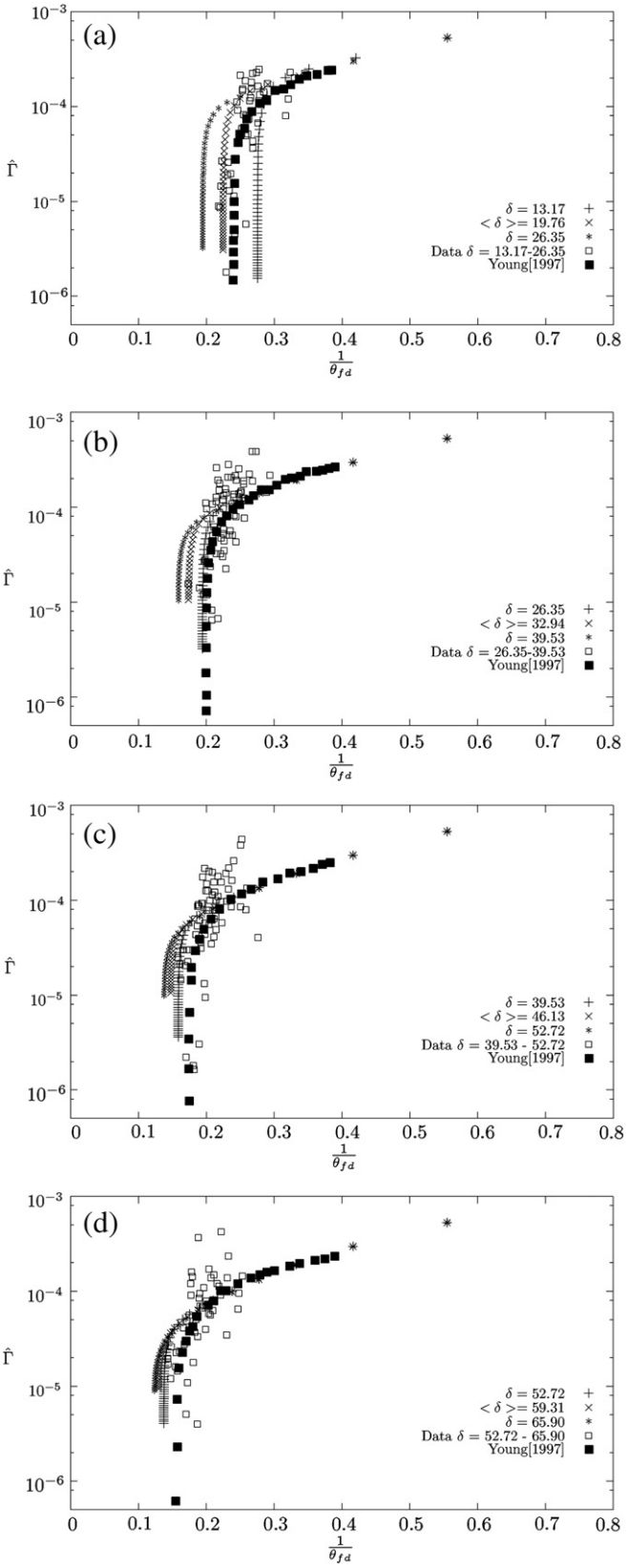

Fig. 3. Growth rate $\hat{\Gamma}$ as a function of inverse wave age $1/\theta_{fd}$ for several values of the parameter δ. White squares correspond to Lake George experiment data, black squares correspond to the empirical relationship (Eq. (6)) found by Young (1997). Present results correspond to symbols +, × and *. (a): the dataset covers a range of wind speed corresponding to $\delta_Y = 0.1 - 0.2$, or, using Eq. (47) $\delta = 13.17 - 26.35$, and an average value $< \delta > = (13.17 + 26.35)/2$ is used. (b): same as (a) with $\delta_Y = 0.2 - 0.3$. (c): same as (a) with $\delta_Y = 0.3 - 0.4$. (d): same as (a) with $\delta_Y = 0.4 - 0.5$.

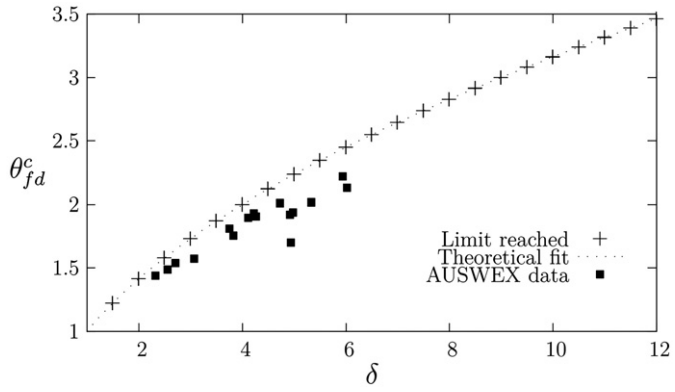

Fig. 4. Parameter curves corresponding to zero growth rate. The theoretical limit is given by Eq. (49). The AUSWEX data are experimental results from Donelan et al. (2006) (the sea state is fairly close to the finite depth full development).

5.2. The wave dissipation influence

This section aims at answering the question: why do the $\hat{\Gamma}$ curves seem to be consistent with the empirical fits of Young (1997), even though bottom friction dissipation (S_{bf}) and white-cap dissipation (S_{ds}) are disregarded?

It is currently admitted that the bottom friction S_{bf} plays a relatively minor role in depth limited growth studies, even though being an important dissipative factor for swell propagating in shallow water (see Young and Babanin, 2006b for more information). Consequently, we do not consider bottom friction in the following analysis. The white-capping dissipation is an important dissipative mechanism since in finite depth conditions, wind waves show significant wave breaking events. Hence, dissipation due to wave breaking S_{ds} is considered to be the dominant dissipative term in finite depth, compared to the deep water case (Young and Babanin, 2006b; Young and Verhagen, 1996a). Now, what can we observe in plots 3(a), 3(b), 3(c) and 3(d)?

- For a constant δ, let us consider $\frac{\delta}{\theta^2_{dw}} = kh \to 0$. This implies that $\frac{1}{\theta_{fd}} \to \frac{1}{\sqrt{\delta}}$, where the wave has reached the point of full development in finite depth. Near this point, we see in Fig. 3(a), (b), (c) and (d) that the $<\delta>$-curves $\hat{\Gamma}$ are above the experimental curves $\hat{\Gamma}_Y$ due to Young (in black squares). This is in line with Fig. 7.1.c in Young (1999), where we see that white-capping dissipation term reaches a maximum damping intensity for kh small, for any peak frequency f_p. Hence, our model overestimates the growth rate value near this point.
- If we consider now, for δ constant, $\frac{\delta}{\theta^2_{dw}} = kh \to \infty$, the waves are in deep water and $\theta_{fd} \sim \theta_{dw} \to 0$. In this case, the curves are merged: $\hat{\Gamma} \sim \hat{\Gamma}_Y$. This agrees with Fig. 7.1.c in Young (1999), where S_{ds} reaches a minimum for deep water at the peak frequency.
- For intermediate regimes, the experimental and theoretical curves are of similar shapes, but $\hat{\Gamma} - \hat{\Gamma}_Y = \epsilon > 0$. The gap size is inversely proportional to the $<\delta>$ value. It can be seen in our plots, as in Fig. 3(a) the gap size is much greater than in and panel (d), where the mean value $<\delta>$ is higher.

From this, we can conclude that disregarding white-capping dissipation in our model led us to an overestimation of the growth rate, in fair agreement with Young (1999). This approach, although qualitative, gives encouraging results: our model appears to be compatible with existing theories of white-cap damping.

6. Conclusion

In this paper our aim is *exclusively* focused on the derivation of a Miles' theory for waves propagating on finite depth h. There are many other parameters that influence the growth of wind-waves in finite depth. For example, wind speed and wind direction variations with time, geometry and bathymetry of the lake, surface drift induced by the air flow, boundary layer turbulence, nonlinear waves interactions, and so on. Taken these into account, all these phenomena represent a work that cannot be handled analytically, even numerically.

Although our study is highly idealized, we believe that it may provide a valuable insight about the effect of depth on the mechanism of water wave amplification by wind and be useful in theoretical forecast of wind-wave growth rates in finite depth.

Acknowledgments

P. M. thanks Labex NUMEV (*Digital and Hardware Solutions, Modelling for the Environment and Life Sciences*) for the partial financial support.

Appendix A. Rayleigh equation

We recall the Rayleigh equation

$$(U-c)\left(\mathcal{W}_a'' - k^2\mathcal{W}_a\right) - U''\mathcal{W}_a = 0 \qquad \forall z \setminus z_0 < z < +\infty \tag{A.1}$$

which is singular in $z_c > z_0 > 0$, where $U(z_c) = c$. This equation underlies one of the most essential mechanism of flow stability. This equation is singular only at zeroth order in s, where $c = c_0 + sc_1$, which is real. The value of c_1, hopefully complex, is then found with the dispersion relation (28). Nevertheless, this is computational, and does not change the fact that we search a complex c eigenvalue in Eq. (A.1). We have to prescribe a flow $U(z)$ allowing instability, or more precisely, not forbidding it. Rayleigh's inflection point theorem, and subsequent Fjortoft theorem states that $U(z)$ is bound to have one inflection point to, at least, not forbid instability (Fjortoft, 1950). Usually, for this theorem, the domain of W_a is $[0, +\infty]$, and the boundary conditions are the vanishing at each bound. But our lower bound is z_0, which is nonzero, and we have a forcing of W_a in z_0. Taking this into account, we derive the following constraint

$$\Im(c)\int_{z_0}^{+\infty} \frac{U''}{|U-c|^2}|\mathcal{W}_a|^2 dz = -\Im\left(\lim_{z\to z_0} \mathcal{W}_a^* \mathcal{W}_a'\right). \tag{A.2}$$

where we see that if $z_0 \to 0$ and W_a vanishes smoothly at the boundaries, considering that $U''(z)$ is monotonous, indeed the r.h.s vanishes and $\Im(c)$ must be zero. Here, it can be nonzero. So, the condition found allows an exponential growth of the free surface $\eta(x,t)$, like a mechanical oscillating system forced into one of its normal modes (Conte and Miles, 1959). We use now a semi-numerical recipe to solve Eq. (A.1) for $\mathcal{W}_a$ following the method introduced by Beji and Nadaoka. We first develop Eq. (A.1) in the z_c-neighborhood, assuming

$$\begin{aligned} &U(z) \approx U'(z_c)(z - z_c) + c, \quad U''(z) \approx U''(z_c), \\ &\left(k\frac{U'(z_c)}{U''(z_c)}\right)^2 \to 0. \end{aligned} \tag{A.3}$$

These are fairly true in the logarithmic wind profile case. After some algebra, these assumptions transform Eq. (A.1) in a Bessel equation of order one, whose solutions are known to be a linear combination of the two first-order Bessel functions. So, with the weighted-centered, dimensionless variable $z_p = -U''(z_c)\frac{(z-z_c)}{U'(z_c)} = \frac{z}{z_c} - 1$ we find

$$\mathcal{W}_a\left(z_p\right) = \sqrt{z_p}\left(C_1 J_1\left(2\sqrt{z_p}\right) + C_2 Y_1\left(2\sqrt{z_p}\right)\right) \tag{A.4}$$

where C_1 and C_2 are complex constants. Here, the function $\mathcal{W}_a$ is z_p-dependent. The numerical solution that we seek can be written as

$$\mathcal{W}_a = C_1 W_1 + C_2 W_2, \tag{A.5}$$

where W_1 and W_2 are unknown and independent. W_1 (resp. W_2) is found by integrating (A.1) with J_1 (resp. Y_1) for initial function value and slope value at z_c. The first step is to avoid the numerical singularity. We achieve this task by introducing a small parameter ε. We choose the two initial points to be $z_c^{\pm} = (1 \pm \varepsilon) z_c$, and evaluate the Bessel functions in these points. As we notice, the function $z_p^{1/2} Y_1(2z_p^{1/2})$ becomes complex, with a negative imaginary part, when $z < z_c$. Its derivative becomes complex, with a positive imaginary part.

We have to take the complex-conjugates of the initial value and initial slope value of these functions to get a positive growth rate[1] (Drazin and Reid, 1982). Therefore, after integration, we get W_1 and W_2. But this does not take into account integration constants. These are set using the boundary conditions of surface forcing and vanishing at infinity. So, using Eq. (A.5) into Eqs. (20) and (21), we obtain a simple algebraic system which allows us to determine C_1 and C_2. The "infinite" value, for computation, is the one from which the constants are stable enough. The relative error on the constants is proportional to the error on the growth rate. Here, a relative error of 10^{-5} is taken. As a result, we obtain $\mathcal{W}_a(z)$, and we can evaluate the integrals in Eq. (37) for any values of the parameters. The results are shown in Fig. 1.

References

Beji, S., Nadaoka, K., 2004. Solution of Rayleigh's instability equation for arbitrary wind profiles. Journal of Fluid Mechanics 500, 65–73.

Belcher, S.E., Hunt, J.C.R., 1993. Turbulent shear flow over slowly moving waves. Journal of Fluid Mechanics 251, 109–148.

Bretschneider, C.L., 1958. Revised wave forecasting relationships. Proc. 6th Conference on Coastal Engineering, Gainsville/Palm Beach/Miami Beach, FL. ASCE, New York, pp. 30–67.

Charnock, H., 1955. Wind stress on a water surface. Quarterly Journal of the Royal Meteorological Society 81, 639–640.

Conte, S.D., Miles, J.W., 1959. On the numerical integration of the orr-sommerfeld equation. Journal of the Society for Industrial and Applied Mathematics 7, 361–366.

Donelan, M.A., Skafel, M., Graber, H., Liu, P., Schwab, D., Venkatesh, S., 1992. On the growth rate of wind-generating waves. Atmosphere-Ocean 30, 457–478.

Donelan, M.A., Babanin, A.V., Young, I.R., Banner, M.L., 2006. Wave-follower field measurements of the wind-input spectral function. Part II: parameterization of the wind input. Journal of Physical Oceanography 36, 1672–1689.

Drazin, P.G., Reid, W., 1982. Hydrodynamic Stability. Cambridge University Press.

Fairall, C.W., Grachev, A.A., Bedard, A., Nishiyama, R.T., 1996. Wind, wave, stress, and surface roughness relationships from turbulence measurements made on r/p flip in the scope experiment. NOAA technical memorandum ERL ETL, 268.

Fenton, J.D., 1979. A high-order cnoidal wave theory. Journal of Fluid Mechanics 94, 129–161.

Fjortoft, R., 1950. Application of integral theorems in deriving criteria of stability of laminar flow and for the baroclinic circular vortex. Geofysiske Publikasjoner 17, 1–52.

Francius, M., Kharif, C., 2006. Three-dimensional instabilities of periodic gravity waves in shallow water. Journal of Fluid Mechanics 561, 417–437.

Garratt, J.R., Hess, G.D., Physick, W.L., Bougeault, P., 1996. The atmospheric boundary layer advances in knowledge and application. Boundary-Layer Meteorology 78, 9–37.

Ijima, T., Tang, F.L.W., 2011. Numerical calculation of wind waves in shallow water. Coastal Engineering Proceedings, North America (URL: https://journals.tdl.org/ICCE/article/view/2401/2076).

Janssen, P.A.E.M., 1991. Quasi-linear theory of wind-wave generation applied to wave forecast. Journal of Physical Oceanography 21, 1631–1642.

Janssen, P.A.E.M., 2004. The Interaction of Ocean Waves and Wind. Cambridge University Press.

Jeffreys, H., 1924. On the formation of waves by wind. Proceedings of the Royal Society of London. Series A: Mathematical and Physical Sciences A107, 189–206.

Jeffreys, H., 1925. On the formation of waves by wind. II. Proceedings of the Royal Society of London. Series A: Mathematical and Physical Sciences A110, 341–347.

Lighthill, M.J., 1978. Waves in Fluids. Cambridge University Press.

Miles, J.W., 1957. On the generation of surface waves by shear ï¬‚ows. Journal of Fluid Mechanics 3, 185–204.

Miles, J.W., 1997. Generation of surface waves by winds. Applied Mechanics Reviews 50–7, R5–R9.

Phillips, O.M., 1957. On the generation of waves by turbulent wind. Journal of Fluid Mechanics 2, 417–445.

Pierson, W.J., Moskowitz, L., 1964. A proposed spectral form for fully developed wind seas based on the similarity theory of s.a. kitaigorodskii. Journal of Geophysical Research 69, 5181–5189.

Rayleigh, L., 1880. On the stability, or instability, of certain fluid motions. Proceedings of the London Mathematics Society XI, 57–70.

Tennekes, H., 1972. The logarithmic wind profile. Journal of the Atmospheric Sciences 30, 234–238.

Thijsse, J.T., 1949. Dimensions of wind-generated waves. General assembly of Association d'Océanographie Physique. Procés-Verbaux 4, 80–81.

Wu, J., 1982. Wind-stress coefficients over sea surface from breeze to hurricane. Journal of Geophysical Research 87, 9704–9706.

Young, I.R., 1997. The growth rate of finite depth wind-generated waves. Coastal Engineering 32, 181–195.

Young, I.R., 1999. Wind Generated Ocean Waves. Elsevier.

Young, I., Babanin, A., 2006a. The form of the asymptotic depth-limited wind wave frequency spectrum. Journal of Geophysical Research 111, C06031. http://dx.doi.org/10.1029/2005JC003398.

Young, I., Babanin, A., 2006b. Spectral distribution of energy dissipation of wind-generated waves due to dominant wave breaking. Journal of Physical Oceanography 36, 376–394.

Young, I.R., Verhagen, L.A., 1996a. The growth of fetch limited waves in water of finite depth. Part I: total energy and peak frequency. Coastal Engineering 29, 47–78.

Young, I.R., Verhagen, L.A., 1996b. The growth of fetch limited waves in water of finite depth. Part II: spectral evolution. Coastal Engineering 29, 79–99.

[1] Taking the non-conjugate values will simply give a minus sign to $\Im(c)$.